ORIGINAL RESEARCH

Translational Insights Into Myocardial Deformation and Fibrosis in Hypertrophic Cardiomyopathy Using Diffusion Tensor MRI



Oumaima Laghzali, MSc,^{a,b,c} Danielle Kara, PhD,^{d,e} Shi Chen, BS,^d Siqin Liu, MD,^{a,b,c} Shahriar Shalikar, MSc,^{a,b} Mara-Camelia Rusu, PhD,^f Fatimunnisa Qadri, PhD,^g Lucie Carrier, PhD,^{h,i} Hsin-Jung Yang, PhD,^j Thoralf Niendorf, PhD,^{a,b,k} Min-Chi Ku, PhD,^{a,c} Christopher Nguyen, PhD^{d,e,l}

ABSTRACT

BACKGROUND Hypertrophic cardiomyopathy (HCM) diagnosis often occurs after myocardium thickening develops, delaying intervention. Cardiac diffusion tensor imaging (cDTI) detects microstructural myocardial remodeling, offering potential for improved risk stratification, especially in patients with preserved ejection fraction.

OBJECTIVES The objective of the study was to determine whether cDTI-derived fractional anisotropy (FA), mean diffusivity, and helix angle (HA) identify myocardial disarray and structural remodeling in HCM in patients and in mouse models.

METHODS Cardiovascular magnetic resonance imaging at 3T with cDTI (FA, mean diffusivity, and HA) and cine imaging was performed in 10 HCM patients with prior late gadolinium enhanced imaging and 10 healthy volunteers. In parallel, 6 myosin binding protein C3-knock-in and 6 wild-type mice (7-8 weeks) underwent cine-cardiovascular magnetic resonance imaging (9.4 T), ex vivo cDTI, scanning electron microscopy, and histology for microstructural, collagen area fraction and fibrosis analysis.

RESULTS HCM patients exhibited reduced FA vs controls $(0.29 \pm 0.03 \text{ vs } 0.34 \pm 0.02; P = 0.002)$, correlating with strain impairment $(R^2 = 0.67; P = 0.003)$ and reaching the lowest value in patients with late gadolinium enhancement (P = 0.02). In knock-in mice, the reduction in FA mirrored the human findings. However, additional alterations were observed, including elevated HA transmurality, significant systolic dysfunction, and a strong correlation between FA and interstitial fibrosis.

CONCLUSIONS FA may reflect critical aspects of myocardial remodeling in HCM, including fibrosis, and mechanical dysfunction, as demonstrated in both preclinical and clinical settings. Its ability to detect abnormalities even in patients with preserved ejection fraction supports its potential as a translational marker for risk stratification and guiding therapeutic intervention. (JACC Adv. 2025;4:102337) © 2025 The Authors. Published by Elsevier on behalf of the American College of Cardiology Foundation. This is an open access article under the CC BY-NC-ND license (http://creativecommons.org/licenses/by-nc-nd/4.0/).

From the ^aMax-Delbrück-Center for Molecular Medicine in the Helmholtz Association (MDC), Berlin Ultrahigh Field Facility (B.U. F.F.), Berlin, Germany; ^bCharité-Universitätsmedizin, Corporate Member of Freie Universität Berlin and Humboldt-Universität zu Berlin, Germany; ^cDZHK (German Centre for Cardiovascular Research), Partner Site BERLIN, Berlin, Germany; ^dCardiovascular Innovation Research Center, Heart Vascular Thoracic Institute, Cleveland Clinic, Cleveland, Ohio, USA; ^eDiagnostic Radiology Cleveland Clinic, Cleveland, Ohio, USA; ^fMax-Delbrück-Center for Molecular Medicine in the Helmholtz Association (MDC), Technology Platform Electron Microscopy, Berlin, Germany; ^gMax-Delbrück-Center for Molecular Medicine in the Helmholtz Association (MDC), Berlin, Germany; ^hDepartment of Experimental Pharmacology and Toxicology, University Medical Center Hamburg-Eppendorf, Hamburg, Germany; ^hDZHK (German Centre for Cardiovascular Research), Partner Site Hamburg/Kiel, Lübeck, Hamburg, Germany; ^hBiomedical Imaging Research Institute, Cedars-Sinai Medical Center, Los Angeles, California, USA; ^kExperimental and Clinical Research Center, Charite Medical Faculty and the Max Delbrueck Center for Molecular Medicine in the Helmholtz Association, Berlin, Germany; and the ^lDepartment of Biomedical Engineering, Case Western Reserve University & Cleveland Clinic, Cleveland, Ohio, USA.

ABBREVIATIONS AND ACRONYMS

CAF = collagen area fraction

cDTI = cardiac diffusion tensor imaging

CMR = cardiovascular magnetic resonance imaging

DTI = diffusion tensor imaging

FA = fractional anisotropy

FOV = field of view

GCS = global circumferential strain

GLS = global longitudinal strain

GRS = global radial strain

HA = helix angle

HAT = helix angle transmurality

HCM = hypertrophic cardiomyopathy

IRB = Institutional Review Board

LA = left atrium

LATEF = left atrium total emptying fraction

LGE = late gadolinium enhancement

LV = left ventricle

LVEF = left ventricular ejection fraction

LVT = left ventricle wall thickening

MD = mean diffusivity

MR = magnetic resonance

MRI = magnetic resonance imaging

Mybpc3 = myosin binding protein C3

SAX = short-axis view

SEM = scanning electron microscopy

SPAIR = spectral adiabatic inversion recovery

TE = echo time

TR = repetition time

WT = wild-type

iffusion tensor imaging (DTI) has substantially advanced cardiac imaging by offering a noninvasive window into the microstructural integrity of myocardial tissues, paving the way for deeper insights into cardiac health and disease. Initially developed for neuroimaging,1 DTI leverages the anisotropic diffusion of water molecules to reveal the orientation and integrity of fibrous structures within tissues, including the myocardium.2 In recent years, its role in cardiac imaging has expanded, particularly in the study of myocardial remodeling.3-5 Cardiac DTI (cDTI) has been shown to map microstructural changes in the border zones of infarcted myocardium, providing a detailed view of postinfarction remodeling.⁶ cDTI is also positioned as a valuable tool in hypertrophic cardiomyopathy (HCM), where the assessment of cardiomyocyte orientation and microstructural integrity is the key unraveling the disease's complex pathophysiology.7,8

cDTI provides several key metrics for assessing myocardial microstructure. Fractional anisotropy (FA) quantifies water diffusion directionality, serving as a proxy of cardiomyocyte organization. Higher FA values indicate well-aligned cardiomyocytes, whereas lower values suggest microstructural disarray, a hallmark of diseases like HCM.9 Mean diffusivity (MD) reflects the overall magnitude of water diffusion, providing information about cell density, water content, and the integrity of cellular membranes. 10 The helix angle (HA) describes the orientation of cardiomyocytes relative to the heart's anatomical axis, which plays a fundamental role in myocardial contraction and relaxation.11

Despite recent contributions to the understanding of myocardial architecture in HCM, 12-14 several key questions remain. The relationship between cDTI parameters, functional impairment, and disease severity

is not yet fully established. The heterogeneity of HCM phenotypes complicates the distinction

between primary microstructural abnormalities and secondary remodeling. A critical gap also exists in correlating cDTI derived metrics with histopathological hallmarks like fibrosis and cardiomyocyte disarray—an insight that could have significant prognostic and therapeutic implications.

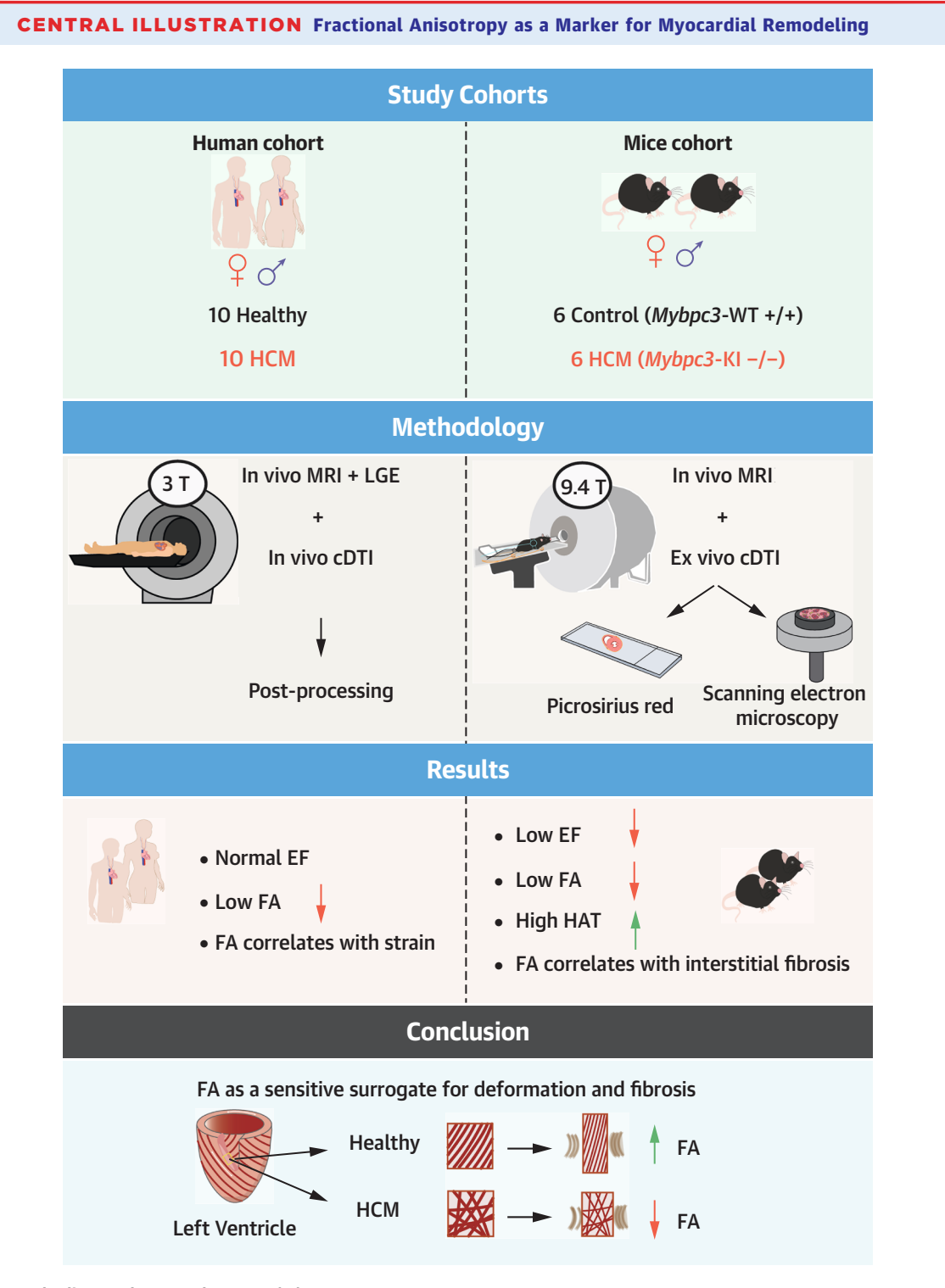
To bridge these gaps, we investigated myocardial microstructural parameters using cDTI in both a human HCM cohort and a well-established HCM mouse model (Central Illustration). In humans, we assessed in vivo cDTI alongside myocardial strain and late gadolinium enhancement (LGE) to evaluate the relationship between diffusion metrics FA, MD, and HA, mechanical function, and fibrotic remodeling. These human findings were then thoroughly validated through cDTI in mice heart specimen. The preclinical model enabled detailed histological validation and mechanistic exploration whereas the human cohort provided direct clinical relevance, enabling us to assess how well animal model findings translate to patients. Through this dual approach, our proof-of-principle investigation provides novel insights into the role of cDTI in detecting and characterizing myocardial abnormalities in HCM and a foundation for its potential clinical application in disease assessment and management.

METHODS

HUMAN COHORT. After approval from the institutional review board at Cleveland Clinic, we conducted magnetic resonance imaging (MRI) scans on a cohort of 10 patients diagnosed with HCM (4 males), all of whom had prior clinical cardiovascular magnetic resonance imaging (CMR) with LGE MRI according to the standard clinical protocols, 15 and the resulting reports were retrospectively accessed with Institutional Review Board approval. LGE reports stated whether patients were LGE+ (presence of LGE) or LGE- (absence of LGE). In the 10-patient cohort, 3 patients were identified as having obstructive HCM and 4 patients were LGE+. Six patients have history of arrythmia, and additional reported symptoms include dyspnea (4), syncope (2), chest pain (4), and fatigue (1). No genotype data were collected.

Moreover, 10 sex and body surface area matched healthy controls (4 males) were included. These scans were performed with an 18-channel body coil

The authors attest they are in compliance with human studies committees and animal welfare regulations of the authors' institutions and Food and Drug Administration guidelines, including patient consent where appropriate. For more information, visit the Author Center.



Laghzali O, et al. JACC Adv. 2025;4(12):102337.

Schematic overview of the study design, methodology, and key findings in human hypertrophic cardiomyopathy (HCM) patients and Mybpc3 knock-in (KI) mice. Human participants underwent in vivo cardiac MRI with late gadolinium enhancement (LGE) and diffusion tensor imaging (cDTI), while mice were studied using ex vivo cDTI, histology and scanning electron microscopy. Results showed reduced fractional anisotropy (FA) in both cohorts, despite preserved ejection fraction (EF) in patients, and low EF in mice. FA correlated with strain in humans and with interstitial fibrosis in mice, while helix angle transmurality (HAT) was increased in HCM mice. Collectively, the findings demonstrate that FA is a sensitive surrogate of myocardial deformation and fibrosis, reflecting microstructural disorganization in HCM $beyond\ conventional\ MRI\ parameters.\ MRI=magnetic\ resonance\ imaging;\ Mybpc3=myosin\ binding\ protein\ C3;\ WT=wild-type.$

on a 3-T magnetic resonance (MR) system (MAGNE-TOM Cima.X; Siemens Healthineers AG), which offers a maximum gradient strength of 200 mT/m at 200 T/m/s. Standard clinical cine MRI was performed in short-axis, 2-chamber, 3-chamber, and 4-chamber views using 2D breath-held, TrueFISP, and retrospective gating to 25 cardiac phases (approximately 360 mm field of view, FOV] and 1.4 mm in-plane spatial resolution with adjustments for body habitus, 8 mm slice thickness). cDTI scans were performed under free-breathing conditions with prospective electrocardiogram triggering for imaging in end systole: 2D radiofrequency ZOOMit diffusion prepared spin echo¹⁶ with second-order motion compensation¹⁷ and spectral adiabatic inversion recovery fat suppression, FOV = 350 mm, matrix = 128×48 , 5 slices short-axis view, 8 mm slice thickness, repetition time (TR) = 5 R-R intervals, 1 reference acquisition at $b = 50 \text{ s/mm}^2$, 8 averages at $b = 500 \text{ s/mm}^2$, 12 diffusion directions (b = 50 s/mm^2 and b = 500 s/mm^2), total scan duration = 540 heartbeats (9 min for a heart rate of 60 bpm). Native T1 and T2 mapping (T1-MOLLI, $FOV = 360 \times 300 \text{ mm}^2$, resolution = 1.4 × 1.4 mm², slice thickness = 8.0 mm, echo time (TE)/TR = 1.0/ 2.5 ms, 5(3)3 acquisition scheme; T2-prepared fast low-angle shot, $FOV = 360 \times 290 \text{ mm}^2$, resolution = $1.8 \times 1.8 \text{ mm}^2$, slice thickness = 8.0 mm, TE/TR = 1.3/3.0 ms, T2 prep durations = [0, 35, 55] ms,3 beat recovery) mapping was acquired in all 10 healthy volunteers and 8 HCM patients.

MOUSE COHORT. All animal studies were approved by the Berlin state review board at the "Landesamt für Gesundheit und Soziales" and conducted in accordance with institutional guidelines. Animal handling and procedures complied with the European Directive 2010/63/EU. The HCM mouse model (myosin binding protein C3-knock-in [Mybpc3-KI]), with a point mutation in the Mybpc3 gene and a C57BL/6J background, was bred and maintained at the Max Delbrück Center for Molecular Medicine in the Helmholtz Association. Heterozygous Mybpc3-KI mice were used to generate homozygous Mybpc3-KI and littermate wild-type (WT) controls. A sample size of 6 WT controls and 6 homozygous Mybpc3-KI mice was chosen to provide 80% power to detect a difference of 1.5 SD in the key CMR parameters at a significance level of 0.05 and is aligned with established practice using mouse models in quantitative CMR techniques. 18-20 Both males and females were used in this study. In total, 3 female and 3 male WT, and 3 female and 3 male homozygous KI mice aged 7 to 8 weeks old were used for in vivo followed by ex vivo experiments. Those homozygous Mybpc3-KI mice develop a robust and well-characterized cardiac phenotype, making them a widely accepted and informative model for studying the pathophysiological mechanisms of HCM.21 The Mybpc3-KI mice exhibited a nonobstructive HCM phenotype characterized by left ventricular hypertrophy and systolic dysfunction, without evidence of arrhythmia. All MR measurements were performed on a 9.4 T small animal MR system (Biospec 94/20) using a 72-mm volume resonator for transmission and a 4-channel surface cardiac radiofrequency array for signal reception. Anesthesia of mice was induced using 3% isoflurane (CP-Pharma) in 300 mL/min medical air and 250 mL/min oxygen, and maintained at 1% to 1.5% isoflurane after induction throughout the imaging. Heart rates, respiration rates, and core body temperature were closely monitored using a monitoring and gating system (Model 1030, SA Instruments Inc). Short-axis view and four-chamber view cine images (intraGate Flash acquisition, $11 \times 22 \text{ mm}^2$ FOV, 57 µm in-plane resolution, 0.8-mm slice thickness, 16 cardiac phases) were obtained in vivo to assess the left ventricular and atrial function.

The mice were then sacrificed while still under anesthesia using cervical dislocation and the hearts were extracted rapidly and placed into ice cold 30 mM KCl until the heart stopped beating. The hearts were then washed 3 times in phosphate-buffered saline and subsequently fixed in paraformaldehyde 4% for 24 hours before being transferred back to phosphate-buffered saline for 48 hours before MRI. Before scanning, the heart chambers were injected with D₂O water to avoid any bubbles (Thermofisher Scientific) and then placed into either 0.5-mL or 1.5-mL Eppendorf tube (depending on heart size) filled with Fomblin (YR-1800, ThermoFisher (Kandel) GmbH) to prevent movement of the sample. Ex vivo cDTI was performed using diffusion sensitized 3D echo planar imaging: TE = 26.4 ms, TR = 2000 ms, spatial resolution = $125 \times 125 \times 306 \,\mu\text{m}$, repetition = 1, receiver bandwidth = 600 kHz, FOV = 19 \times 17 \times 11 mm, matrix = $154 \times 136 \times 36$, slice = 11 mm, averages = 7, $b = 3,000 \text{ s/mm}^2$, b0 directions = 5, diffusiondirections = 30, scan time = 4 h 54 min.

COLLAGEN AREA FRACTION. Paraffin-embedded coupes of WT and KI mouse hearts ($n = 12, 5 \mu m$) were deparaffinized in xylene followed by a rehydration of 100, 96, 80, 70, and 50% ethanol. The sections were then incubated in 0.1% picrosirius red solution (Sigma-Aldrich) for 1 h. Excess staining was cleared by washing with 0.01 mol/L HCl and dehydrated by incubation with 80, 96, and 100% ethanol. Samples

were then incubated in xylene and coversliped with xylene based mounting medium Eukit. Tissues were imaged on a brightfield microscope (BZ-X800, Keyence). Per heart, a minimum of 18 images were analyzed with ImageJ (National Institutes of Health) to determine the mean ratio of interstitial fibrosis to tissue size (collagen area fraction [CAF]).

Z-DISC OFFSET. Post MRI scans, the left ventricular free wall of all mice hearts was fixed in glutaraldehyde, then sectioned and processed for scanning electron microscopy (SEM) to enable ultrastructural assessment, ²² including Z-disc offset measurement to evaluate potential disarray and misalignment near intercalated discs. After tissue preparation and SEM, micrographs were captured at a pixel size of 4.5 nm/pixel. These images were used to measure Z-disc offset by drawing a line perpendicular to a row of sarcomeres near the intercalated discs. The offset of 10 rows of Z-discs relative to this reference line was measured. The distances between the Z-discs and the reference line were recorded, and the mean value for each mouse was calculated and compared between genotypes.

MR IMAGING ANALYSIS. Cardiac chamber quantification from cine imaging was performed using the open-source software Segment (v4.0 R11044b, Medviso, segment.heiberg.se).23 Manual segmentations of the left ventricle (LV) and left atrium (LA) were used to assess cardiac function. Total LA emptying fraction was calculated as follows (left atrial total emptying fraction [LATEF] in %): 100 × (LAVmax - LAVmin)/LAVmax through segmentation of the left atrium on a 4-chamber view and 2-chamber view cine images, where LAVmax and LAVmin are the LA volumes right before the mitral valve opens and right after the mitral valve closes, respectively. Myocardial strain was evaluated using advanced feature tracking,24 enabling precise quantification of regional myocardial deformation by tracking specific myocardial points across multiple cardiac cycles and slices. Longitudinal, radial, and circumferential strain parameters were analyzed, with strain values expressed as the percent change in myocardial segment length relative to its original length.

All postprocessing for cDTI was performed in Python using an in-house custom-built library.²⁵ For the human cohort, respiratory motion correction of the diffusion weighted images was performed before tensor fitting with multitasking respiratory motion correction.¹⁶ Pixelwise MD, FA, and HA were calculated using eigen analysis. Global MD, FA, and HA transmurality (HAT) values were calculated over the entire LV based on manual segmentations.

STATISTICAL ANALYSIS. All experimental statistics and graphs were generated in R studio (R Studio Inc).

For the human cohort, normality was assessed using a Shapiro-Wilk test. Variance homogeneity was assessed using the Levene test. Based on these results, we applied the following: Welch t-test or independent t-test for between-group comparisons, selected according to variance homogeneity; Pearson correlation for normally distributed variables; Mann-Whitney U test for non-normally distributed variables; and Spearman rank correlation when normality assumptions were violated. For the mouse cohort, given the limited sample size of 12 mice and some non-normally distributed variables, we exclusively applied nonparametric statistical approaches. Correlation strength was defined as: very weak (0.00-0.19), weak (0.20-0.39), moderate (0.40-0.59), strong (0.60-0.79), and very strong (0.80-1.00). All results were presented as mean \pm SD values with statistical significance set at P < 0.05.

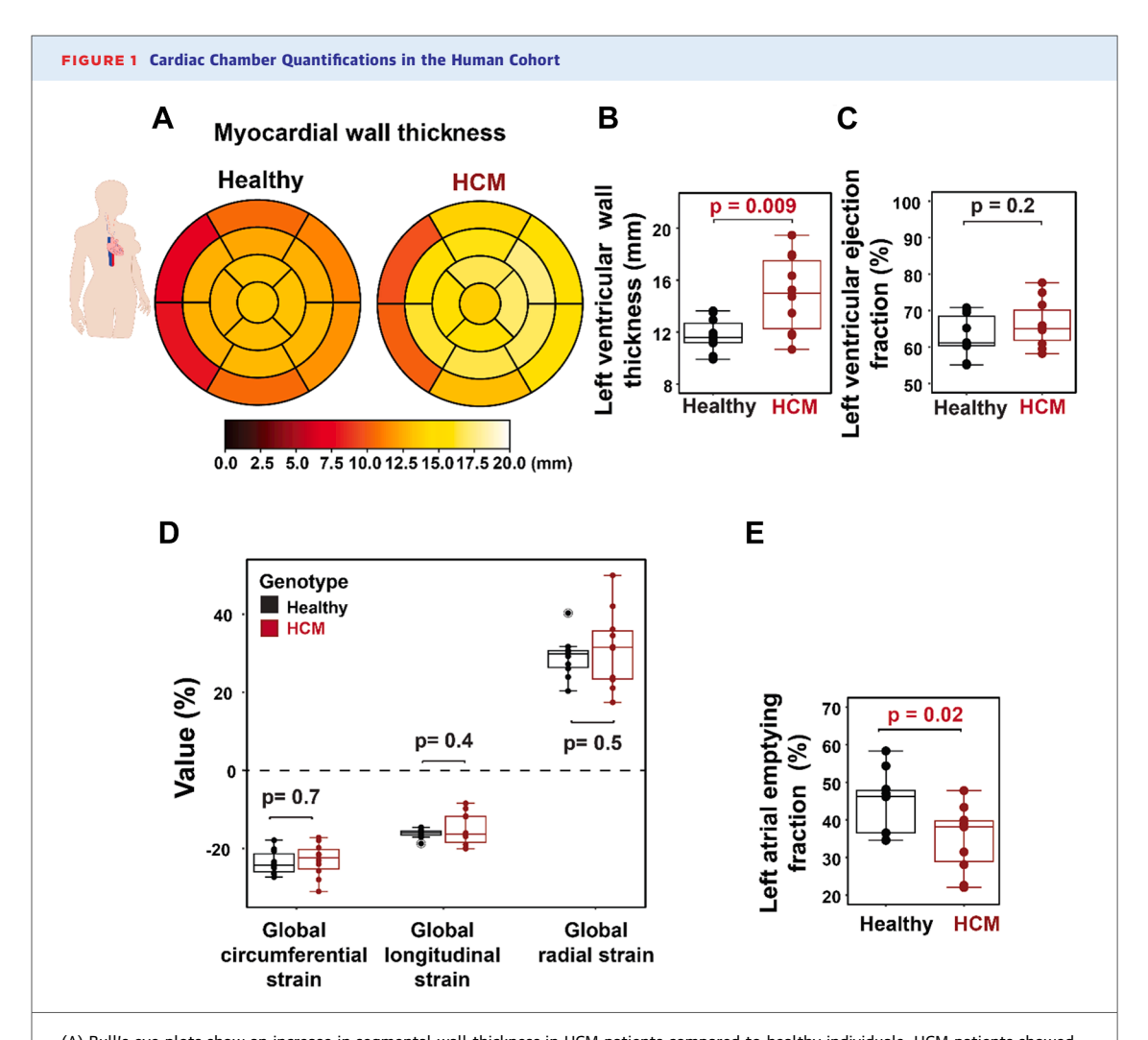
RESULTS

CARDIAC CHAMBER QUANTIFICATION AND MR FEATURE TRACKING REVEAL DIASTOLIC DYSFUNCTION IN HCM PATIENTS. Twenty subjects were included in this study: 10 with HCM and 10 healthy volunteers. All cohort characteristics are described in Table 1, whereas Figure 1 shows cardiac chamber quantifications results. Bull's eye plots based on American Heart Association 17-segment model illustrated segmental wall thickness in HCM patients with a more uniform increase in the apical, lateral, anterior, and inferior regions (Figure 1A). HCM patients showed highly significant LV wall thickening (LVT) compared to the healthy subjects (LVT $_{HCM}$ = $14.94 \pm 2.98 \text{ mm}$; LVT_{Healthy} = $11.77 \pm 1.27 \text{ mm}$; P = 0.009) (Figure 1B). Despite these structural differences, HCM patients had a preserved left ventricular ejection fraction (LVEF) with no significant difference between the HCM group and the healthy counterparts (LVEF $_{HCM}$ = 66.35% \pm 6.48%, $LVEF_{Healthy} = 62.93\% \pm 5.77\%, P = 0.2$) (Figure 1C). We assessed strain in our cohort to reflect changes in myocardial systolic deformation. No significant differences were found between groups in global circumferential strain (GCS), global longitudinal strain (GLS), or global radial strain (GRS) (P value = 0.73, 0.41, and 0.57, respectively) (Figure 1D). To assess diastolic function, we evaluated the LATEF and revealed a significant difference in LATEF between HCM and healthy (LATEFHCM: $35.06\% \pm 8.67\%$, LATEF_{Healthy}: $44.25\% \pm 8.41\%$, P = 0.02) (Figure 1E).

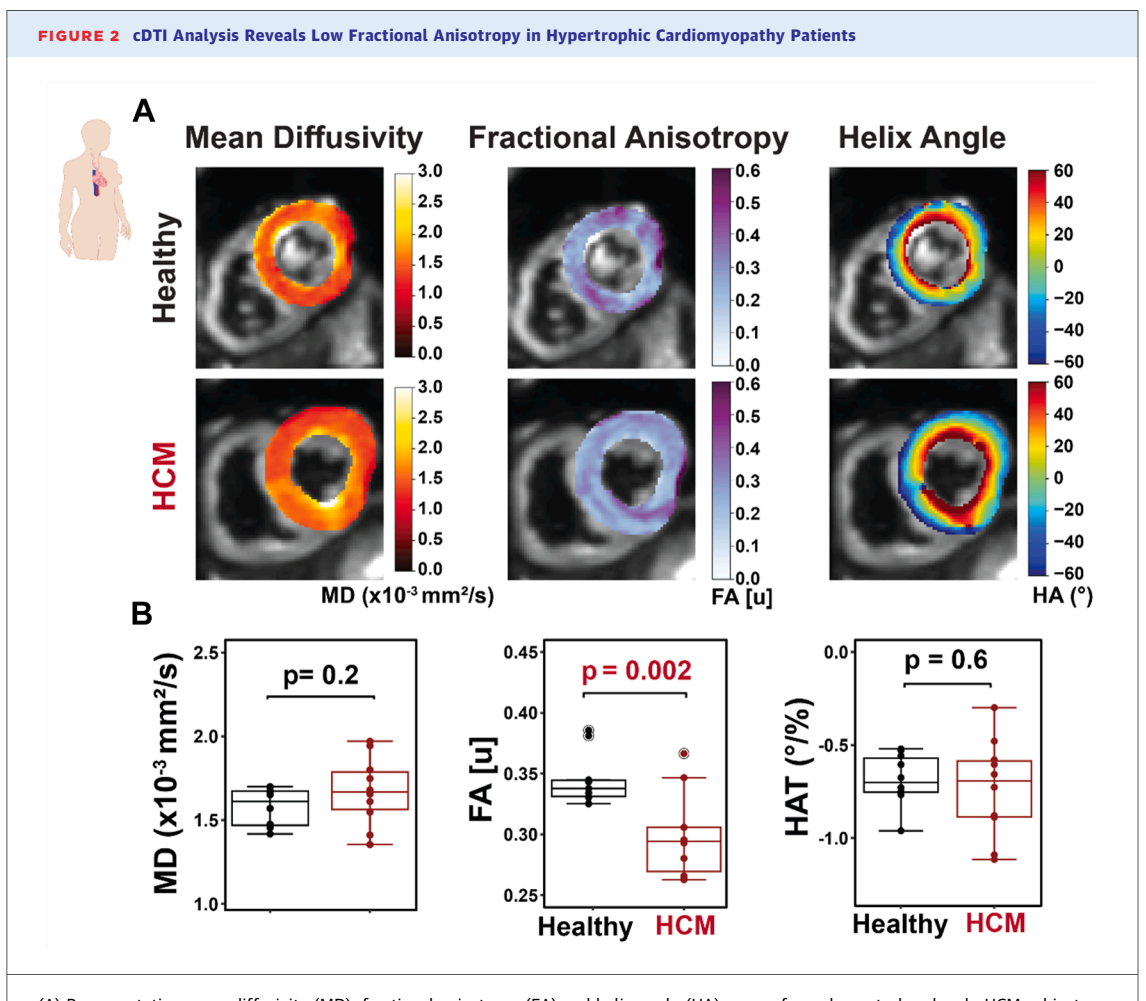
Characteristic	Human Cohort			Mouse Cohort		
	Healthy	нсм	P Value	WT	KI	P Value
Male, n	10 (4)	10 (4)	1.00	6 (3)	6 (3)	1.00
Age (years/weeks)	46.9 ± 12	58.6 ± 12	0.05	7.33 \pm 0.51 wk	7.16 \pm 0.40 wk	0.59
BSA (m ²)	1.9 ± 0.2	1.98 ± 0.2	0.89	0.006 ± 0.0005	0.006 ± 0.001	1.00
LVMi (g/m²)	59.8 ± 10.0	77.6 ± 18.9	0.02	11.5 ± 1.54	19.2 ± 3.51	0.004
LVEDVi (mL/m²)	84.8 ± 20.2	73.9 ± 11.0	0.17	6.64 ± 1.61	11.08 ± 3.51	0.09
LVESVi (mL/m ²)	31.5 ± 9.0	25.1 ± 6.7	0.10	1.95 ± 0.64	8.03 ± 2.88	0.002
SVi (mL/m ²)	53.3 ± 13.5	48.9 ± 7.1	0.40	4.69 ± 1.01	3.04 ± 1.03	0.01
COi (L/min/m²)	3.4 ± 1.1	3.1 ± 0.5	0.67	2.46 ± 0.45	1.71 ± 0.66	0.02
HR (bpm)	62.2 ± 10.5	65.07 ± 8.6	0.65	444.83 ± 12.65	443.66 ± 7.39	0.81

Cardiac chamber quantification was performed for the study cohorts, followed by group comparisons with corresponding P values reported. Values are mean \pm SD, with P values <0.05 considered statistically significant and shown in **bold**.

BSA = body surface area; COi = cardiac output index; HCM = hypertrophic cardiomyopathy; HR = heart rate; KI = knocked-in; LVEDVi = left ventricular end diastolic volume index; LVESVi = left ventricular end systolic volume index; LVMi = left ventricular mass index; SVi = stroke volume index; WT = wild-type.



(A) Bull's eye plots show an increase in segmental wall thickness in HCM patients compared to healthy individuals. HCM patients showed significantly (B) increased LV maximal wall thickness, whereas (C) left ventricular ejection fraction remains unchanged. (D) Comparison of global circumferential strain, longitudinal strain, and radial strain showing no significant differences in strain values across groups, whereas (E) left atrial emptying fraction is reduced in HCM patients compared to controls. HCM = hypertrophic cardiomyopathy.



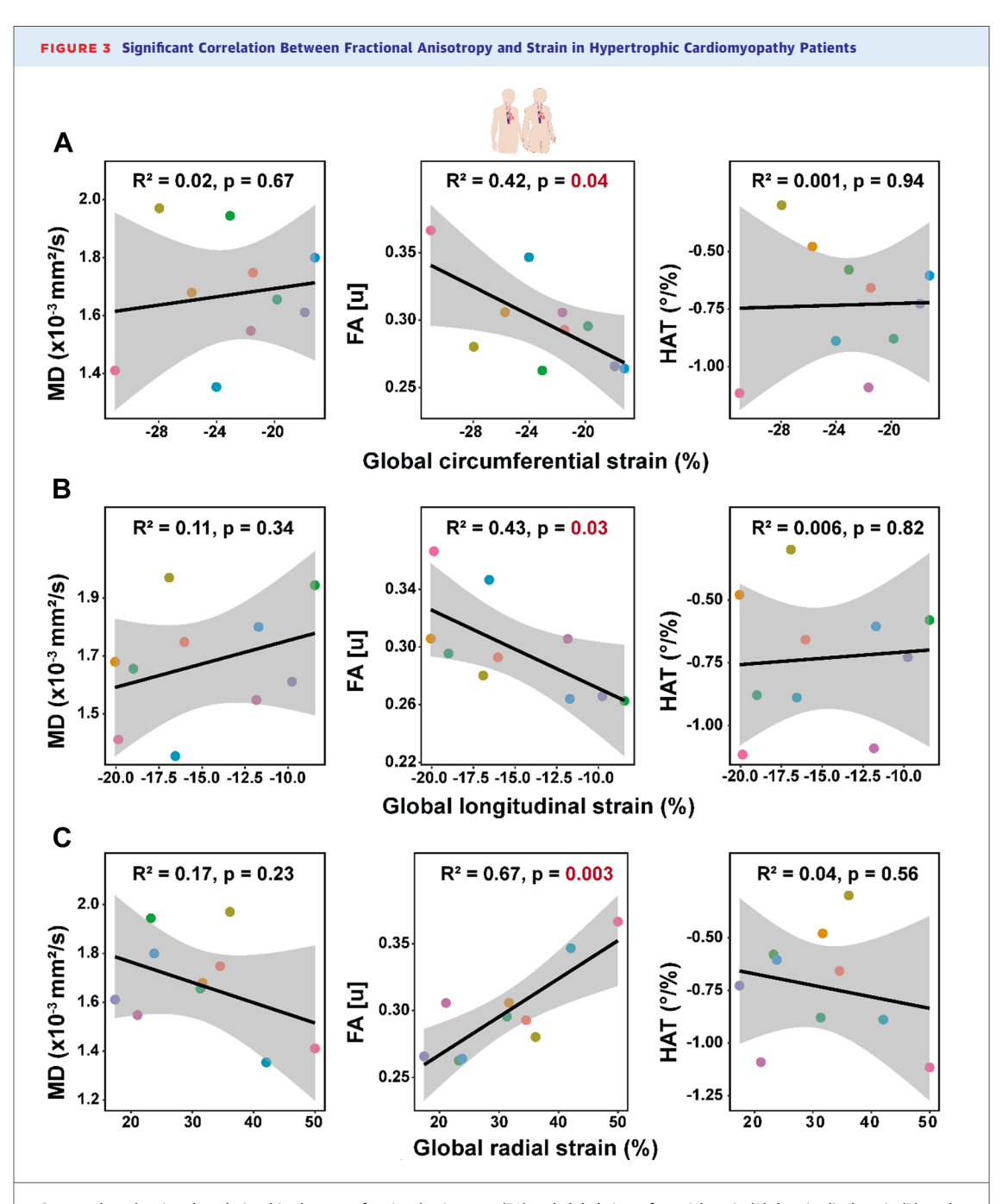
(A) Representative mean diffusivity (MD), fractional anisotropy (FA) and helix angle (HA) maps of a male control and male HCM subject.
(B) cDTI shows lower FA in HCM patients but no significant difference in MD or HAT vs healthy controls. Abbreviations as in Figure 1.

CDTI DETECTS CHANGES IN FA IN HCM PATIENTS WITH PRESERVED EJECTION FRACTION. cDTI analysis revealed significantly lower global FA values in HCM patients (FA $_{HCM}$ = 0.29 \pm 0.03 vs $\mathrm{FA_{Healthy}} = 0.34 \pm 0.02$, P = 0.002) (Figure 2B). Global HAT and MD values did not significantly differ between the 2 groups (HAT_{HCM} = $-0.73 \pm 0.26^{\circ}$ /%, $HAT_{Healthy} = -0.68 \pm 0.13^{\circ}/\%$, P = 0.62 and $MD_{HCM}~=~1.67~\pm~0.20~\times~10^{-3}~mm^2/s,~MD_{Healthy}~=$ $1.57 \pm 0.11 \times 10^{-3} \text{ mm}^2/\text{s}, P = 0.21$). Linear relationships between FA and myocardial strain were observed exclusively in HCM subjects (Figures 3A to **3C**). Specifically, FA showed moderate correlations with circumferential ($R^2 = 0.42$, P = 0.04) and longitudinal strain ($R^2 = 0.43$, P = 0.03) and a strong correlation with radial strain ($R^2 = 0.67$, P = 0.003).

ATED WITH FA IN HCM PATIENTS. All HCM patients underwent LGE assessment. Among HCM patients,

we stratified individuals based on the presence or absence of LGE (Figure 4B). Both LGE+ and LGE- groups included male and female patients, without apparent sex-based differences in LGE prevalence. FA was significantly lower in LGE + patients than in LGE- patients (P = 0.02) Figure 4C.

SEVERE CARDIAC MORPHOLOGICAL AND STRAIN ABNORMALITIES ARE SHOWN IN OUR MURINE HCM MODEL. In vivo cardiac assessment of 12 mice (6 WT and 6 KI) revealed pronounced structural and functional abnormalities in KI mice. Bull's eye plots demonstrated pronounced regional hypertrophy in KI mice, especially in the apical and lateral walls (**Figure 5A**). KI mice showed significantly higher LVT (LVT_{KI} = 1.31 \pm 0.16 mm, LVT_{WT} = 0.89 \pm 0.06 mm, P = 0.002) (**Figure 5B**), along with lower LVEF (LVEF_{KI} = 17.64% \pm 2.86%, LVEF_{WT} = 64.77% \pm 7.79%, P = 0.002) (**Figure 5C**). Strain analysis confirmed systolic dysfunction, with markedly lower GCS, GLS, and

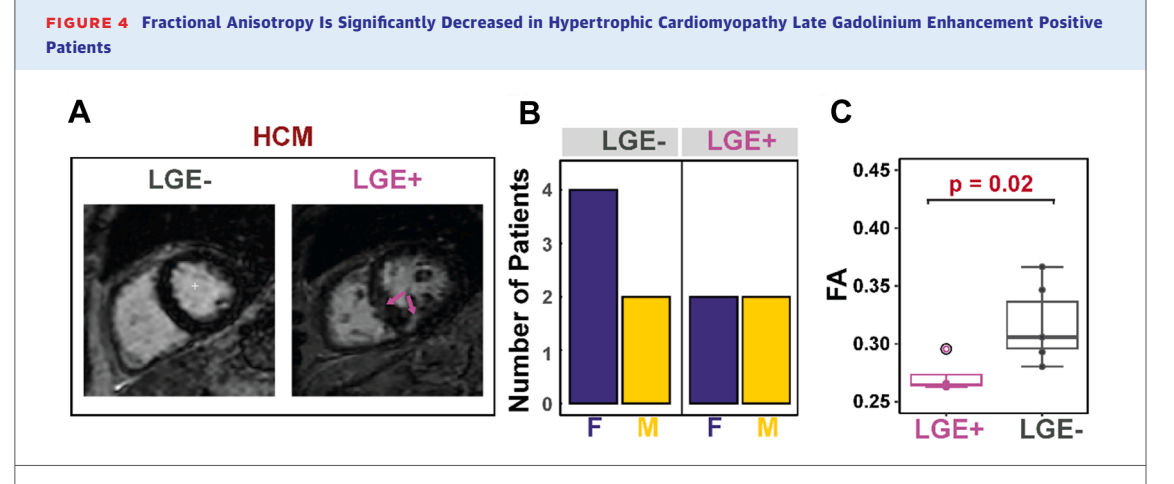


Scatter plots showing the relationships between fractional anisotropy (FA) and global circumferential strain (A), longitudinal strain (B), and radial strain (C) for HCM patients (n = 10) demonstrated significant correlations. In contrast, no significant correlations were observed between Helix angle transmurality (HAT) or mean diffusivity (MD) and any strain parameters. Linear regression lines with shaded CIs are shown, with corresponding R^2 and P values indicating the strength and significance of the associations.

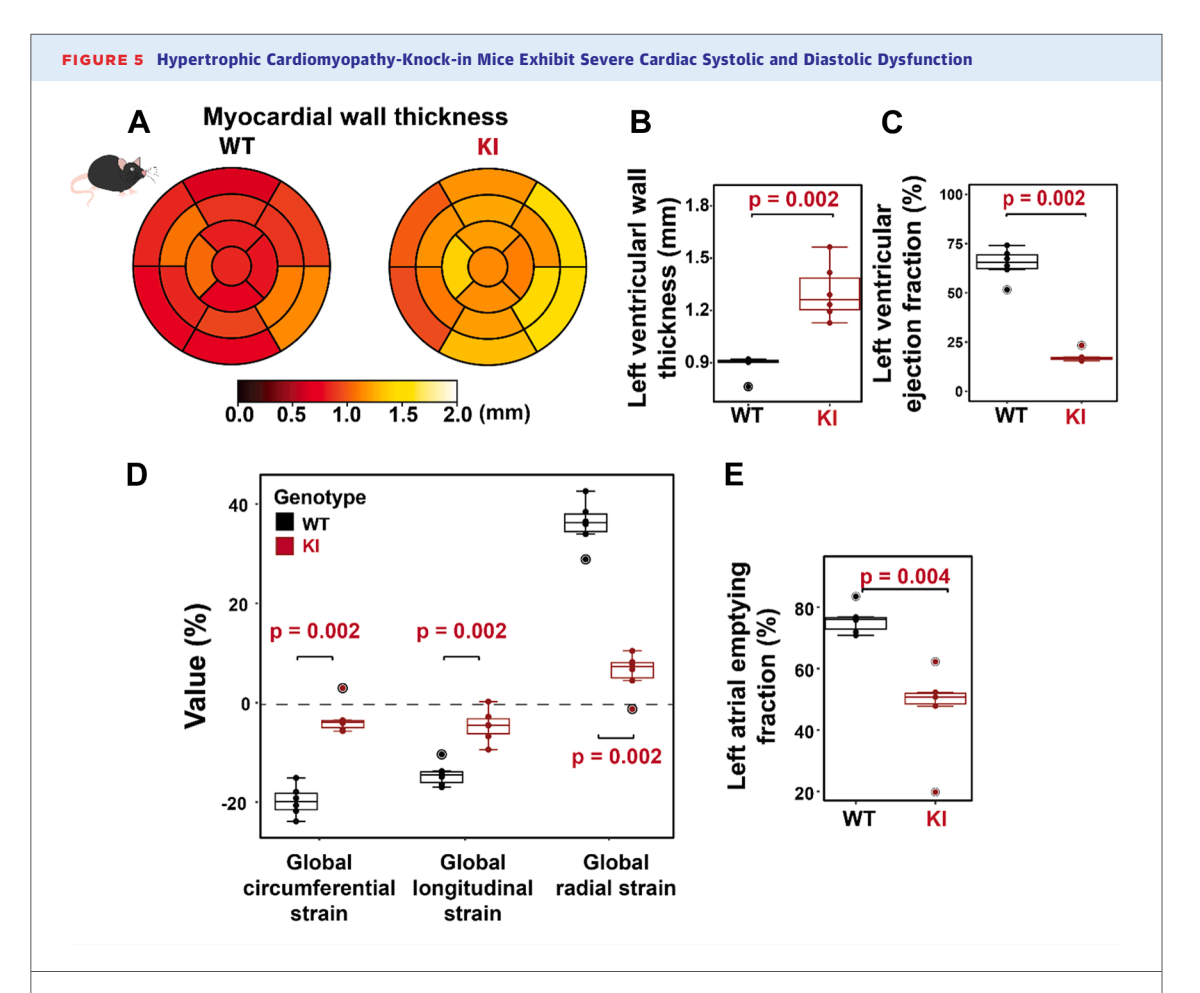
GRS in KI mice (GCS_{KI} = $-3.25\% \pm 3.16\%$, GCS_{WT} = $-19.76\% \pm 3.06\%$, P = 0.002; GLS_{KI} = $-4.63\% \pm 3.30\%$, GLS_{WT} = $-14.46\% \pm 2.35\%$, P = 0.002; GRS_{KI} = $6.05\% \pm 4.08\%$, GRS_{WT} = $36.04\% \pm 4.57\%$, P = 0.002) (Figure 5D). Consistent with human findings,

LATEF was also significantly lower in KI mice, highlighting impaired atrial function (LATEF $_{\rm KI}$: 47.25% \pm 14.34%, LATEF $_{\rm WT}$: 75.81% \pm 4.47%, P=0.004) (**Figure 5E**). More mouse cohort characteristics are provided in **Table 1**.

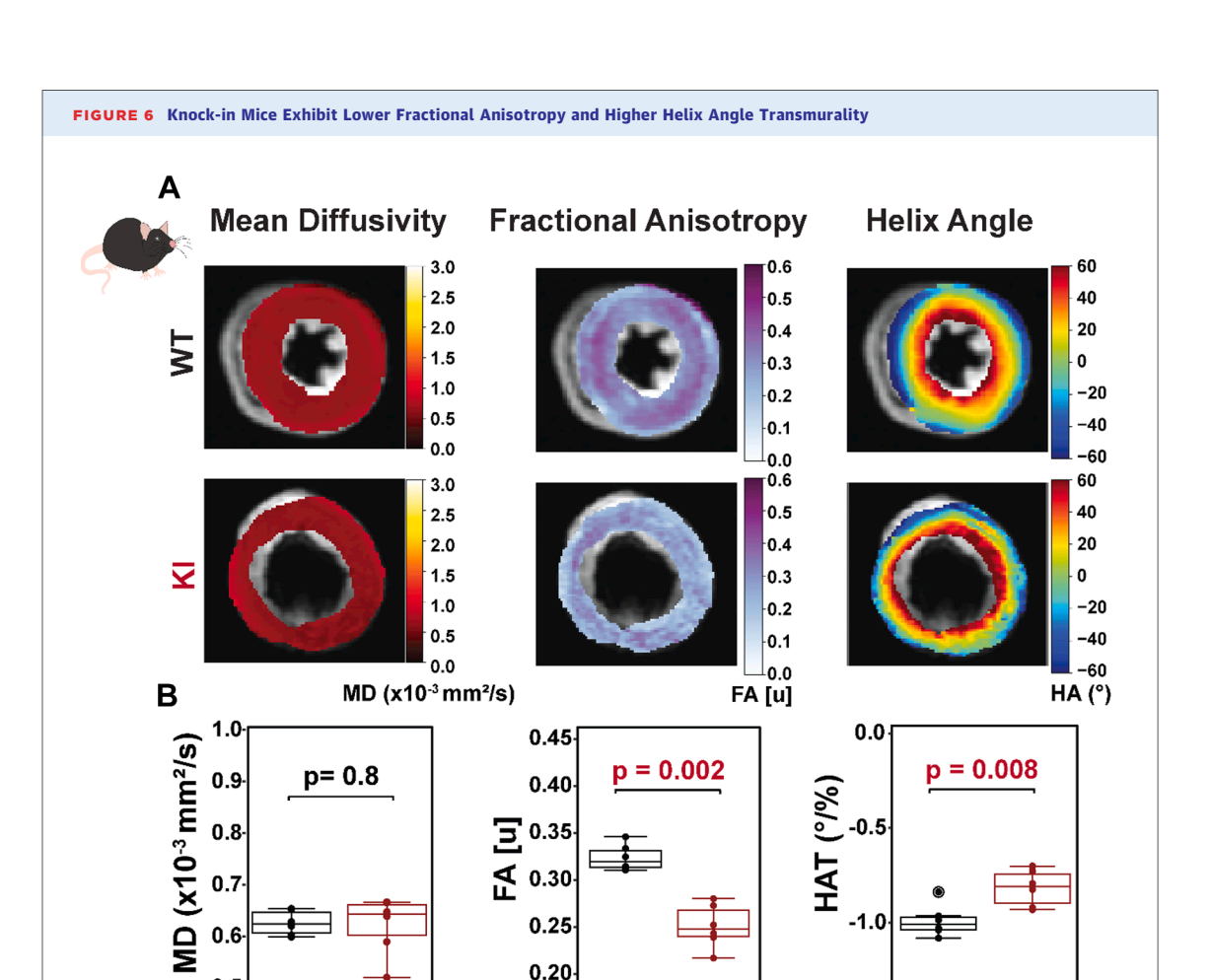
9



(A) Representative images of an LGE-male subject (left) and an LGE + male subject (right) with arrows highlighting myocardial focal fibrosis in the HCM heart. (B) Distribution of LGE-negative (LGE-) and LGE-positive (LGE+) patients by sex. (C) Comparison of FA (mean \pm SEM) between LGE+ and LGE- groups. LGE = late gadolinium enhancement; other abbreviation as in Figure 1.



KI mice exhibit (A) a uniform increase in segmental wall thickness, with more pronounced thickening in the lateral segments, (B) significantly increased left ventricular wall thickness, and (C) reduced left ventricular ejection fraction. (D) Strain analysis reveals significant reductions in strain. (E) Left atrial emptying fraction is significantly decreased in KI mice. KI = knock-in; WT = wild-type.



(A) Representative maps of mean diffusivity (MD), fractional anisotropy (FA), and helix angle (HA) in female wild-type (WT) and knocked-in (KI) mice and (B) boxplots confirming reduced FA and elevated helix angle transmurality (HAT) in KI mice compared to control.

WT

FA THAT CORRELATE WITH FIBROSIS MARKERS IN MICE. Figure 6 shows significantly lower global FA values and higher HAT values in KI mice $(FA_{KI} = 0.25 \pm 0.02, FA_{WT} = 0.32 \pm 0.01, P = 0.002$ and $HAT_{KI} = -0.83 \pm 0.09^{\circ}/\%$, $HAT_{WT} = -1.00 \pm 0.08^{\circ}/\%$, P = 0.008). However, global MD did not significantly differ between groups $(MD_{KI} = 0.62 \pm 0.05 \times 10^{-3} \text{ mm}^2/\text{s}$, $MD_{WT} = 0.62 \pm 0.02 \times 10^{-3} \text{ mm}^2/\text{s}$, P = 0.81). When correlating the cDTI-derived parameters with myocardial strain in mice (**Figure 7**), no significant associations were observed for MD and HAT. Although FA exhibited trends similar to those seen in humans, these did not reach statistical significance.

EX VIVO cDTI REVEALS SIGNIFICANT CHANGES IN

0.5

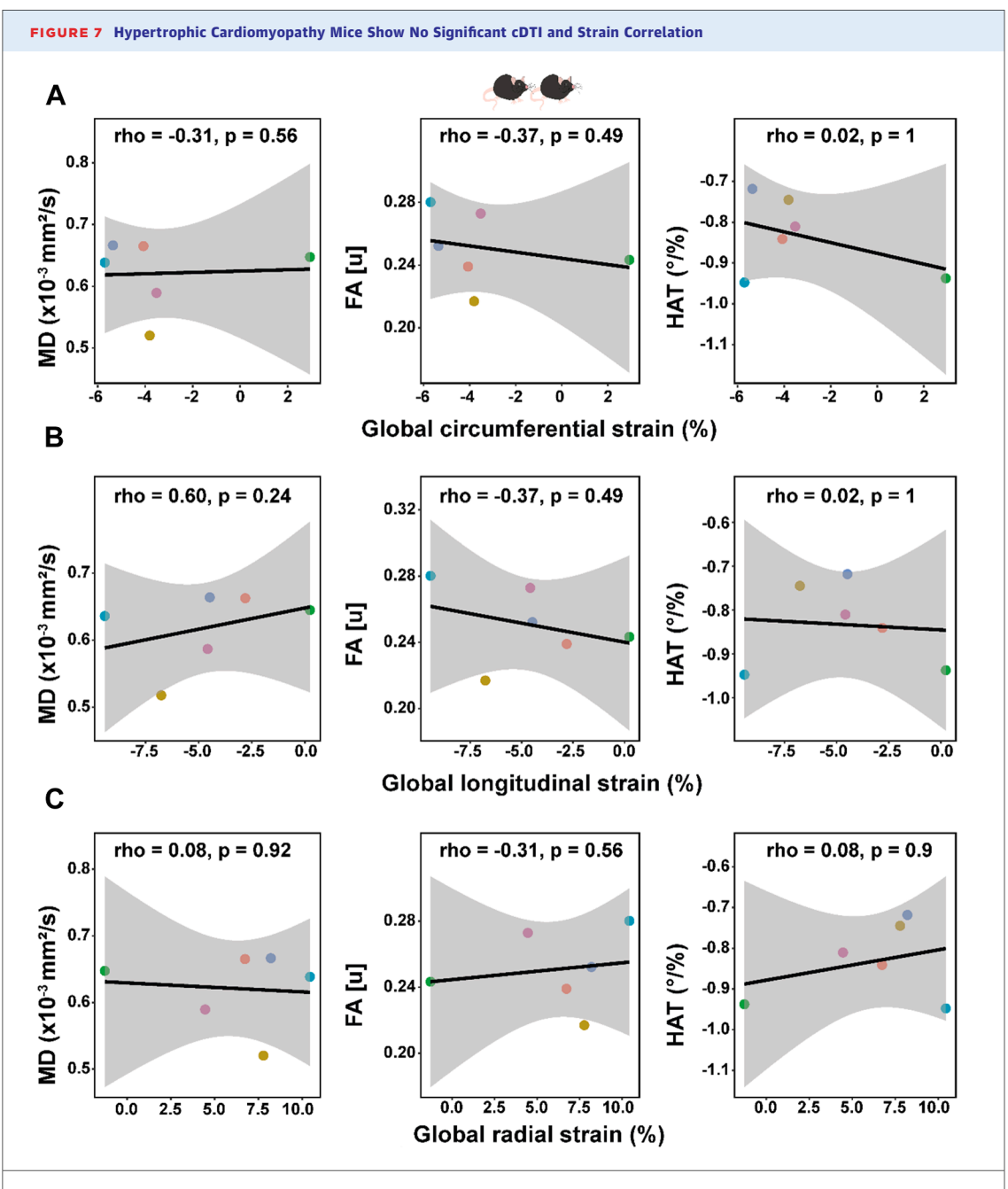
Post-CMR histology revealed subtle ultrastructural and fibrotic differences between groups. Z-disc offset was mildly higher in KI mice without reaching statistical significance (Offset $_{\rm KI}=0.56~\pm~0.15~\mu m$ vs

Offset $_{\rm WT}=0.44\pm0.11~\mu m,~P=0.05$), though qualitative SEM analysis showed regional cardiomyocyte disarray in KI mice (Figure 8A). The relationship between cDTI parameters and Z-disc offset measurements did not reach statistical significance in our mice cohort (Figure 8B). Picrosirius red staining demonstrated significantly increased interstitial fibrosis in KI mice, with higher CAF (CAF $_{\rm KI}=8.85\pm1.65\%$ vs CAF $_{\rm WT}=5.12\%\pm1.35\%,~P=0.002$) (Figure 8C ii). Notably, FA values showed a strong negative correlation with CAF (rho = -0.79, P=0.003), indicating a strong relationship between FA and histologically confirmed fibrosis.

WT

DISCUSSION

Our translational study provides important insights into myocardial deformation and fibrosis in HCM by integrating cDTI in HCM patients and mice. Building

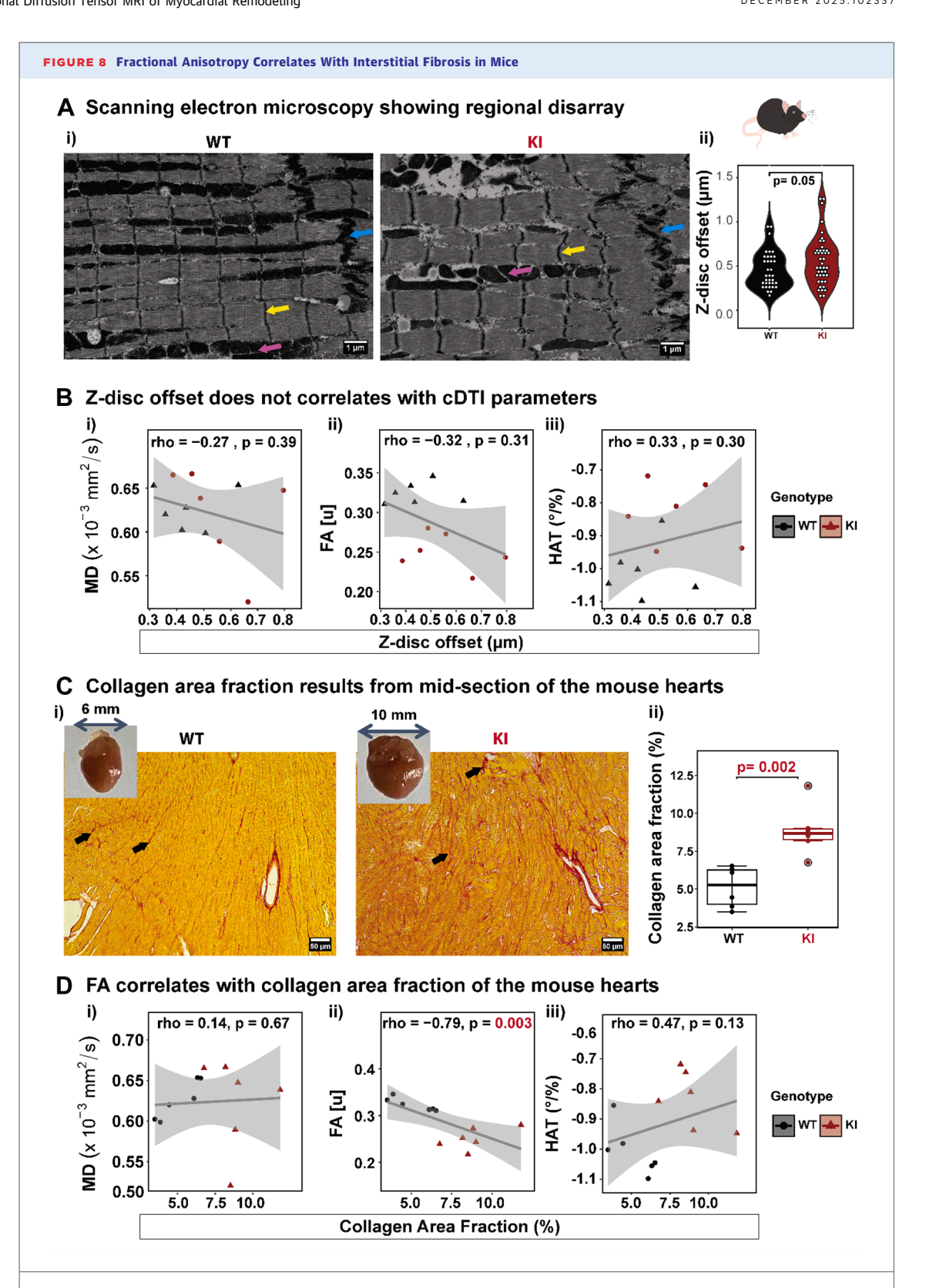


Scatter plots showing the relationships between mean diffusivity (MD), fractional anisotropy (FA), Helix angle transmurality (HAT) and (A) global circumferential strain, (B) longitudinal strain, and (C) radial strain for HCM mice (n = 6) showing no significant correlations. Linear regression lines with shaded CIs are shown, with corresponding rho and P values indicating the strength and significance of the associations.

on observations made in humans, we aimed to validate and further explore these findings in mice. Our findings suggest that FA may serve as a sensitive marker for detecting myocardial fibrotic remodeling in HCM, particularly among individuals with preserved ejection fraction.

MICROSTRUCTURAL PATHOLOGY IN HCM

Our study demonstrates that FA, derived from cDTI, is significantly reduced in HCM patients with preserved LVEF compared to healthy controls. The reduction was most pronounced in patients with



(A-i) Scanning electron microscopy reveals regional myocyte disarray in KI mice compared to WT controls (Color-coded arrows: yellow = Z-disc, magenta = mitochondria, blue = intercalated disc), (A-ii) with quantification of Z-disc offset not showing a significant increase in KI. (B i-iii) No significant correlations have been found between cDTI parameters and Z-disc offset. (C i-ii) Picrosirius red staining of mid-sections of mouse hearts demonstrate increased collagen deposition (black arrows) in KI compared to WT. (D i-iii) Correlation analysis between cDTI parameters and collagen area fraction reveals strong negative correlation with fractional anisotropy (FA). cDTI = cardiac diffusion tensor imaging; HAT = Helix angle transmurality; MD = mean diffusivity; other abbreviations a sin Figure 5.

LGE, supporting a link between FA and fibrotic remodeling. This aligns with previous studies showing associations between reduced FA, LGE burden, and arrhythmogenic risk in HCM.²⁶ Although decreased FA and its association with LGE could be related to extracellular edema,27 no significant differences were observed in T2 mapping between HCM patients and controls (Supplemental Figure 1), nor was FA significantly correlated with T2 in the HCM cohort (Supplemental Figure 2). Because increased T2 has been linked to myocardial edema,²⁸ these results support the observed decrease in FA as a reflection of fibrotic content rather than edema. To further explore these findings, we investigated a severe form of HCM using the Mybpc3-KI mouse model. This model showed pronounced functional impairment, mild fibrosis, and reduced FA values at an early age, and was used as a positive control for comparison with the human population. In contrast to LGE in humans, which primarily reflects focal replacement fibrosis, our mouse model enabled direct assessment of interstitial fibrosis, revealing a strong correlation between FA and fibrotic burden. These results are consistent with prior work demonstrating that low FA reflects key histopathological features of HCM, including interstitial fibrosis and cardiomyocyte disarray. 13,14 Furthermore, FA abnormalities have been reported even in subclinical HCM, suggesting that microstructural changes, particularly disarray, may precede overt functional impairment.^{29,30} However, in our mouse model, ultrastructural analysis of Z-disc disarray did not correlate with FA. This may suggest that interstitial fibrosis is the predominant contributor to diffusion abnormalities in this context. These findings underscore the complex interplay between fibrosis and disarray in HCM pathology, where their combined influence may shape the diffusion signal captured by cDTI.3,31 This interpretation is supported by developmental studies indicating that fibrosis and disarray co-emerge early in HCM progression, 32,33 and that their interaction may lead to a nonlinear remodeling of myocardial microstructure, ultimately reflected in parameters such as FA.

Although FA showed robust differences, other cDTI metrics such as MD and HAT, did not differ significantly between HCM patients and controls, echoing previous findings for HAT.²⁶ The absence of MD elevation contrasts with earlier studies,¹⁴ potentially reflecting differences in cohort characteristics or disease stage, underscoring the complex interplay between microstructure and diffusion behavior. Together, these findings suggest that FA may be useful as a sensitive, contrast-free imaging

marker of myocardial remodeling in HCM-even in the presence of preserved ejection fraction—and highlight the complex, stage-dependent contributions of fibrosis and disarray to diffusion abnormalities.

FUNCTIONAL ASSESSMENT BEYOND LVEF. HCM patients in our study exhibited marked LV hypertrophy despite preserved LVEF, reinforcing the limitations of relying on LVEF alone. Importantly, both human and mouse data consistently demonstrated reductions in LATEF, reinforcing its value as a sensitive marker of diastolic dysfunction, even in the setting of preserved LVEF in humans.³⁴ In the human cohort, global strain parameters (GCS, GLS, and GRS) were not significantly different at the group level compared to healthy controls. However, FA showed a strong correlation with strain. Mechanistically, this suggests that reduced directional coherence of cardiomyocytes compromises the efficiency of myocardial deformation. Interestingly, this correlation between FA and strain was not observed in our KI mice, despite the fact that strain was significantly impaired in the KI group. Several hypotheses could explain this discrepancy. First, the presence of altered HAT in KI mice may influence the relationship between FA and strain. Second, differences in imaging methodology-namely, the use of in vivo cDTI in humans vs ex vivo cDTI in mice-may also affect the sensitivity of diffusion metrics to physiological motion. Future studies employing in vivo cDTI in mouse models will be crucial to disentangle these potential confounders and clarify the relationship between FA and functional performance across species.

Despite these species-specific differences, the reproducibility of FA abnormalities across both models underscores its potential as a noninvasive, quantitative marker of myocardial remodeling. Although FA alone cannot fully capture the complexity of myocardial pathology, when interpreted alongside complementary imaging markers and clinical data, it enables a more robust and specific myocardial characterization. By capturing fibrosis and its functional consequences, FA may offer a valuable addition to the current toolkit for assessing disease severity and progression in HCM.

STUDY LIMITATIONS. This study is limited by the relatively small sample size in both human and mouse cohorts, although significant differences were still detected, highlighting the sensitivity of cDTI metrics. No genetic testing was performed in the human cohort. The absence of genetic testing in human subjects precluded direct comparison with the *Mybpc3* mutation studied in mice; however, given

the high prevalence of *Mybpc3* genetic variants in HCM, the model remains highly relevant.³³ The KI mouse model was selected as a validated HCM phenotype with reproducible microstructural alterations, as no currently available homozygous mouse model fully recapitulates the human HCM phenotype, which is characterized by diastolic dysfunction with preserved or enhanced systolic function. Future studies should incorporate genetic screening in patients and more comprehensive histopathological analyses in mice—including assessment of microvascular dysfunction, myocyte remodeling, and extracellular matrix reorganization—to better define the structural basis of functional changes and their association with FA.

CONCLUSIONS

This study suggests that FA, derived from cDTI, may serve as a sensitive imaging marker of myocardial changes in HCM, detectable even in patients with preserved function and minimal strain abnormalities. In our mouse model, FA reduction was similarly observed alongside more severe functional decline, suggesting conserved microstructural changes across species. Correlations between FA, fibrosis, and strain highlight the link between structural remodeling and functional impairment. These findings support FA as a potential surrogate marker for fibrotic remodeling. Future research should aim to standardize cDTI protocols, validate FA thresholds, and integrate human and preclinical data to improve early diagnosis, risk stratification, and targeted therapy in HCM.

ACKNOWLEDGMENTS The authors thank Saskia Schlossarek (Pharmacology Institute, University Medical Center Hamburg-Eppendorf, Hamburg, Germany) for providing the HCM mouse model.

FUNDING SUPPORT AND AUTHOR DISCLOSURES

Funding sources include National Institutes of Health (R01HL151704, R01EB033853, and R01HL159010). This study is also supported by the German Research Foundation (DFG: CA 618/9-1; KU 3722/4-1; WA 2804/7-1). The authors have reported that they have no relationships relevant to the contents of this paper to disclose.

ADDRESS FOR CORRESPONDENCE: Dr Min-Chi Ku, Berlin Ultrahigh Field Facility (B.U.F.F.), Max Delbrück Center for Molecular Medicine in the Helmholtz Association (MDC), Robert-Rössle Strasse 10, Berlin 13125, Germany. E-mail: min-chi.ku@mdc-berlin.de.

PERSPECTIVES

clinical practice.

COMPETENCY IN MEDICAL KNOWLEDGE: This proof-of-principle investigation suggests that FA, derived from cDTI, can noninvasively detect myocardial remodeling even in HCM patients with preserved cardiac function and no significant strain abnormalities. FA also correlates with fibrosis and myocardial strain, suggesting it reflects both structural and functional remodeling in HCM. These findings position FA as a promising marker for earlier diagnosis and more refined risk stratification in

TRANSLATIONAL OUTLOOK: Our findings support the clinical promise of cDTI and FA in the early detection and monitoring of HCM and may provide new insights into microstructural changes before overt functional deterioration. Future studies should pursue longitudinal imaging-pathology correlations, assess the predictive value of FA in patient outcomes, and explore its role in guiding personalized therapeutic strategies in HCM.

REFERENCES

- **1.** Chen B, Moreland J, Zhang J. Human brain functional MRI and DTI visualization with virtual reality. *Quant Imaging Med Surg*. 2011;1(1):11-16. https://doi.org/10.3978/j.issn.2223-4292.2011. 11.01
- **2.** Pashakhanloo F, Herzka DA, Mori S, et al. Submillimeter diffusion tensor imaging and late gadolinium enhancement cardiovascular magnetic resonance of chronic myocardial infarction. *J Cardiovasc Magn Reson*. 2017;19(1):9. https://doi.org/10.1186/s12968-016-0317-3
- **3.** Nguyen C, Lu M, Fan Z, Bi X, Kellman P, Zhao S, Li D. Contrast-free detection of myocardial fibrosis in hypertrophic cardiomyopathy patients with diffusion-weighted cardiovascular magnetic

- resonance. *J Cardiovasc Magn Resonance*. 2015; 17(1):107. https://doi.org/10.1186/s12968-015-0214-1
- **4.** Axel L, Wedeen VJ, Ennis DB. Probing dynamic myocardial microstructure with cardiac magnetic resonance diffusion tensor imaging. *J Cardiovasc Magn Reson.* 2014;16(1):89. https://doi.org/10.1186/s12968-014-0089-6
- **5.** Mekkaoui C, Reese TG, Jackowski MP, Bhat H, Sosnovik DE. Diffusion MRI in the heart. *NMR Biomed*. 2017;30(3):e3426. https://doi.org/10.1002/nbm.3426
- **6.** Kung GL, Vaseghi M, Gahm JK, Shevtsov J, Garfinkel A, Shivkumar K, Ennis DB. Microstructural infarct border zone remodeling in the post-

infarct swine heart measured by diffusion tensor MRI. Front Physiol. 2018;9:826. https://doi.org/10.3389/fphys.2018.00826

- **7.** Fattal J, Henry MA, Ou S, et al. Magnetic resonance imaging of hypertrophic cardiomyopathy: beyond left ventricular wall thickness. *Can Assoc Radiol J.* 2015;66(1):71–78. https://doi.org/10.1016/j.carj.2014.07.005
- **8.** Khalique Z, Scott AD, Ferreira PF, Nielles-Vallespin S, Firmin DN, Pennell DJ. Diffusion tensor cardiovascular magnetic resonance in hypertrophic cardiomyopathy: a comparison of motion-compensated spin echo and stimulated echo techniques. *MAGMA*. 2020;33(3):331-342. https://doi.org/10.1007/s10334-019-00799-3

- **9.** Tseng WY, Dou J, Reese TG, Wedeen VJ. Imaging myocardial fiber disarray and intramural strain hypokinesis in hypertrophic cardiomyopathy with MRI. *J Magn Reson Imaging*. 2006;23(1): 1–8. https://doi.org/10.1002/jmri.20473
- **10.** Khalique Z, Ferreira PF, Scott AD, Nielles-Vallespin S, Firmin DN, Pennell DJ. Diffusion tensor cardiovascular magnetic resonance imaging: a clinical perspective. *JACC Cardiovasc Imaging*. 2020;13(5):1235-1255. https://doi.org/10.1016/j.jcmg.2019.07.016
- 11. Nguyen CT, Buckberg G, Li D. Magnetic resonance diffusion tensor imaging provides new insights into the microstructural alterations in dilated cardiomyopathy. *Circ Cardiovasc Imaging*. 2016;9(10). https://doi.org/10.1161/CIRCIMAG-ING.116.005593
- **12.** Lee SE, Nguyen C, Yoon J, Chang HJ, Kim S, Kim CH, Li D. Three-dimensional cardiomyocytes structure revealed by diffusion tensor imaging and its validation using a tissue-clearing technique. *Sci Rep.* 2018;8(1):6640. https://doi.org/10.1038/s41598-018-24622-6
- **13.** Das A, Chowdhary A, Kelly C, et al. Insight into myocardial microstructure of athletes and hypertrophic cardiomyopathy patients using diffusion tensor imaging. *J Magn Reson Imaging*. 2021;53 (1):73–82. https://doi.org/10.1002/jmri.27257
- **14.** Das A, Kelly C, Teh I, et al. Phenotyping hypertrophic cardiomyopathy using cardiac diffusion magnetic resonance imaging: the relationship between microvascular dysfunction and microstructural changes. *Eur Heart J Cardiovasc Imaging*. 2022;23(3):352–362. https://doi.org/10.1093/ehjci/jeab210
- **15.** Kellman P, Arai AE. Cardiac imaging techniques for physicians: late enhancement. *J Magn Resonance Imaging*. 2012;36(3):529-542. https://doi.org/10.1002/jmri.23605
- **16.** Nguyen CT, Christodoulou AG, Coll-Font J, et al. Free-breathing diffusion tensor MRI of the whole left ventricle using second-order motion compensation and multitasking respiratory motion correction. *Magn Reson Med.* 2021;85(5): 2634–2648. https://doi.org/10.1002/mrm.28611
- **17.** Stoeck CT, von Deuster C, Genet M, Atkinson D, Kozerke S. Second-order motion-compensated spin echo diffusion tensor imaging of the human heart. *Magn Reson Med*. 2016;75(4): 1669-1676. https://doi.org/10.1002/mrm.25784
- **18.** Pereda D, García-Lunar I, Sierra F, et al. Magnetic resonance characterization of cardiac adaptation and myocardial fibrosis in pulmonary

- hypertension secondary to systemic-topulmonary shunt. *Circ Cardiovasc Imaging*. 2016;9(9):e004566. https://doi.org/10.1161/ CIRCIMAGING.116.004566
- **19.** Faragli A, Tanacli R, Kolp C, et al. Cardiovascular magnetic resonance feature tracking in pigs: a reproducibility and sample size calculation study. *Int J Cardiovasc Imaging*. 2020;36(4):703-712. https://doi.org/10.1007/s10554-020-01767-y
- **20.** Lapinskas T, Grune J, Zamani SM, et al. Cardiovascular magnetic resonance feature tracking in small animals a preliminary study on reproducibility and sample size calculation. *BMC Med Imaging*. 2017;17(1):51. https://doi.org/10.1186/s12880-017-0223-7
- 21. Fraysse B, Weinberger F, Bardswell SC, et al. Increased myofilament Ca2+ sensitivity and diastolic dysfunction as early consequences of Mybpc3 mutation in heterozygous knock-in mice. *J Mol Cell Cardiol*. 2012;52(6):1299–1307. https://doi.org/10.1016/j.yjmcc.2012.03.009
- **22.** Liu S, Laghzali O, Shalikar S, Rusu MC, Carrier L, Niendorf T, Ku MC. Cardiac MRI strain as an early indicator of myocardial dysfunction in hypertrophic cardiomyopathy. *Int J Mol Sci.* 2025;26(4):1407.
- 23. Heiberg E, Sjogren J, Ugander M, Carlsson M, Engblom H, Arheden H. Design and validation of Segment-freely available software for cardiovascular image analysis. *BMC Med Imaging*. Jan 11 2010;10(1). https://doi.org/10.1186/1471-2342-10-1
- **24.** Queiros S, Morais P, Barbosa D, Fonseca JC, Vilaca JL, D'Hooge J. MITT: medical image tracking toolbox. *IEEE Trans Med Imaging*. Nov 2018;37(11):2547-2557. https://doi.org/10.1109/TMI.2018.2840820
- **25.** Kara D, Liu Y, Chen S, et al. In vivo cardiac diffusion tensor imaging on an MR system featuring ultrahigh performance gradients with 200 mT/m maximum gradient strength. *Magn Reson Med.* 2025;93(2):673–688. https://doi.org/10.1002/mrm.30308
- **26.** Ariga R, Tunnicliffe EM, Manohar SG, et al. Identification of myocardial disarray in patients with hypertrophic cardiomyopathy and ventricular arrhythmias. *J Am Coll Cardio*. 2019;73(20):2493–2502. https://doi.org/10.1016/j.jacc.2019.02.065
- **27.** Amano Y, Tachi M, Tani H, Mizuno K, Kobayashi Y, Kumita S. T2-weighted cardiac magnetic resonance imaging of edema in myocardial diseases. *ScientificWorldJournal*. 2012;2012: 194069. https://doi.org/10.1100/2012/194069

- **28.** Stoeck CT, von Deuster C, Fuetterer M, et al. Cardiovascular magnetic resonance imaging of functional and microstructural changes of the heart in a longitudinal pig model of acute to chronic myocardial infarction. *J Cardiovasc Magn Resonance*. 2021;23(1):103. https://doi.org/10.1186/s12968-021-00794-5
- 29. Joy G, Kelly CI, Webber M, et al. Evidence for microstructural alteration and microvascular disease in subclinical and overt hypertrophic cardiomyopathy. Eur Heart J Cardiovasc Imaging. 2023;24(Supplement_1). https://doi.org/10.1093/ehjici/jead119.099
- **30.** Joy G, Kelly CI, Webber M, et al. Microstructural and microvascular phenotype of sarcomere mutation carriers and overt hypertrophic cardiomyopathy. *Circulation*. 2023;148(10):808–818. https://doi.org/10.1161/CIRCULATIONAHA.123.
- **31.** Abdullah OM, Drakos SG, Diakos NA, et al. Characterization of diffuse fibrosis in the failing human heart via diffusion tensor imaging and quantitative histological validation. *NMR Biomed*. 2014;27(11):1378–1386. https://doi.org/10.1002/nbm.3200
- **32.** Garcia-Canadilla P, Cook AC, Mohun TJ, et al. Myoarchitectural disarray of hypertrophic cardiomyopathy begins pre-birth. *J Anatomy*. 2019;235(5):962–976. https://doi.org/10.1111/ioa.13058
- **33.** Hilderink S, Schuldt M, Goebel M, et al. Characterization of heterozygous and homozygous mouse models with the most common hypertrophic cardiomyopathy mutation MYBPC3(c. 2373InsG) in the Netherlands. *J Mol Cell Cardiol*. 2023;185:65–76. https://doi.org/10.1016/j.yjmcc. 2023.10.008
- **34.** Farhad H, Seidelmann SB, Vigneault D, et al. Left atrial structure and function in hypertrophic cardiomyopathy sarcomere mutation carriers with and without left ventricular hypertrophy. *J Cardiovasc Magn Reson.* 2017; 19(1):107. https://doi.org/10.1186/s12968-017-0420-0

KEY WORDS diffusion, fractional anisotropy, hypertrophic cardiomyopathy, microstructure, mouse model, MRI

APPENDIX For supplemental figures, please see the online version of this paper.